RESEARCH PAPER

Acta Neurobiol Exp 2026, 86: 63–75
DOI: 10.55782/z4j0rp75

Microglia up-regulate thromboxane A2 synthesis genes in response to C6 glioma-conditioned medium

Michał Dąbrowski[1]*, Beata Kaza[1], Bartłomiej Gielniewski[2], Bartosz Wojtaś[2], Bożena Kamińska[1], Marta Maleszewska[3]

[1] *Laboratory of Molecular Neurobiology, Nencki Institute of Experimental Biology, Polish Academy of Sciences, Warsaw, Poland*
[2] *Laboratory of Sequencing, Nencki Institute of Experimental Biology, Polish Academy of Sciences, Warsaw, Poland*
[3] *Department of Animal Physiology, Institute of Experimental Zoology, Faculty of Biology, University of Warsaw, Warsaw, Poland*
** Email: m.dabrowski@nencki.edu.pl*

Microglia accumulate in malignant gliomas and play a pivotal role in tumor progression. Using single-cell RNA sequencing studies researchers have probed gene expression in the myeloid cells in experimental gliomas at relatively late stages of the tumor development. Therefore, the early changes in gene expression in microglia in response to glioma are not fully characterized. We have previously reported distinct profiles of gene expression in the rat primary microglia cultures treated for 6 hours with either rat C6 glioma-conditioned medium (GCM) or lipopolysaccharide. In the current study, using RNA-seq, we characterized the transcriptional response of rat primary microglia to GCM *in vitro* at different time-points: 6 h, 24 h, and 48 h, as compared to the control treated for 6 h with its own medium. We observed that during the GCM treatment gene expression changes in a biphasic, swing-like pattern. This includes the genes involved in innate immune response, which are mostly down-regulated at 6 h by the GCM treatment, as compared to the time-matched control, and subsequently up-regulated at 48 h, as compared to the earlier time-points of the GCM treatment. Conversely, the genes involved in the cell cycle are up-regulated at 6 h and down-regulated at 48 h, which coincides with the induction of *Tgfb1*. Notable exceptions to this biphasic pattern include key genes activating immune response, such as *Tlr9* and *Myd88*, which are down-regulated early and persistently, while genes inhibiting immune activation, such as *Trem1*, and genes involved in a metabolic switch, such as *Pfkl*, are persistently up-regulated. Most notably, the up-regulated genes include *Ptgs1* (alias *Cox1*) and *Tbxas1*, which encode the enzymes catalyzing the synthesis of thromboxane A2, a known inducer of T cell suppression. Further studies are needed to test the functional consequences of their up-regulation.

Key words: microglia expression profiling, RNA-seq, C6 glioma-conditioned medium, rat

INTRODUCTION

Glioblastoma wild type IDH (GBM) is the primary, WHO grade 4 brain tumor. Despite surgery, radio- and chemotherapy GBM patients have a poor prognosis. GBMs are infiltrated by myeloid cells, which constitute up to 30-40% of the tumor mass. The composition of glioma-associated myeloid cells (GAMs) changes while the tumor progresses. Initially, the tumor becomes infiltrated by the microglia – central nervous system (CNS) resident myeloid cells (Gabrusiewicz et al., 2011). Due to this different ontogeny, as microglia originate from yolk sac progenitors, colonize the CNS during early embryogenesis, and persist throughout the entire life (Prinz et al., 2014), these cells display distinct transcriptional signature from peripheral macrophages (Butovsky et al., 2014). Microglia associated with malignant gliomas are polarized into immunosuppressive, tumor supporting cells (Gieryng et al., 2017b ; Buonfiglioli & Hambardzumyan, 2021). In the murine GL261 gliomas at day 7 after the implantation, the myeloid cells that accumulate at the tumor site are predominantly activated microglia (Gabrusiewicz et al., 2011; Sielska et al., 2013; Virtuoso et al., 2022). The changes

Received 5 December 2025, accepted 24 March 2026

in gene expression in glioma-associated myeloid cells (GAMs) as well as their subpopulations have been characterized by using single-cell RNA sequencing (scRNA-seq) (Bowman et al., 2016; Ochocka et al., 2021, 2023; Pombo Antunes et al., 2021). The cytokines and chemokines secreted by tumor-associated microglia stimulate a massive influx of the monocytes into the brain from the blood, which is observed at day 14 (Gabrusiewicz et al., 2011). These monocytes undergo differentiation into macrophages and by day 21 acquire high levels of immunosuppressive markers, such as Arg1 and PD-L1, which are absent in blood monocytes (Ochocka et al., 2023). In human glioma patients, microglia-derived GAMs were predominant in newly diagnosed tumors, but were outnumbered by monocyte-derived GAMs following recurrence, especially in hypoxic tumor environments (Pombo Antunes et al., 2021). Recurrent high grade gliomas are characterized by a prominent infiltration of immature dendritic cells and immunosuppressive macrophages (Roura et al., 2021).

The above studies point to the pivotal role of microglia during early stages of glioma development. However, the activation of microglia in response to the factors released by tumor cells is not fully understood. Available *in vivo* single cell RNA studies probed gene expression in the myeloid cells inside the glioma either at a single, late time-point of 21 days (Ochocka et al., 2021; Pombo Antunes et al., 2021), or at several time-points – days 14 and 21 (Ochocka et al., 2023). A milestone study (Kirschenbaum et al., 2024) utilizing Zman-seq method demonstrated that the process of polarization of incoming monocytes into immunosuppressive macrophages is completed within 48 hours. However, the Zman-seq technique is not applicable to microglial cells, as it relies on pulse-labelling of peripheral blood cells.

We previously reported transcriptomic changes in the rat primary microglia cells *in vitro* treated for 6 hours with either microglia-conditioned medium (MGCM), rat C6 glioma-conditioned medium (GCM) or lipopolysaccharide (LPS), determined by microarray gene expression analysis (Ellert-Miklaszewska et al., 2013). Distinct patterns of changes in gene expression induced by either treatment were revealed. Genes, such as *Nos2* and *Il1b* were induced by the LPS treatment only, while other genes, including *Arg1*, *Cx3cr1*, *Id1*, *Myc*, *Smad7*, were preferentially induced by the GCM treatment. The GCM treatment also affected chromatin openness of rat primary microglial cells at the 6 h time-point (Przanowski et al., 2019), and induced changes in the histone modification pattern (Maleszewska et al., 2021).

In the current study we characterized the transcriptional response of rat primary microglia to GCM *in vitro* at 3 time-points: 6 h, 24 h, and 48 h, and compared to the control (being microglia exposed for 6 h to MGCM). We demonstrate that a majority of genes involved in the innate immune response are down-regulated at 6 h by the GCM treatment, as compared to the MGCM control, and then are up-regulated at 48 h, as compared to the earlier time-points of the GCM treatment. The exceptions to this pattern, include the two genes *Ptgs1* and *Tbxas1,* encoding the enzymes catalyzing the synthesis of thromboxane A2 (TXA2), a known inducer of T cell suppression, which are stably up-regulated in microglia at 6 h and 48 h of the GCM treatment.

METHODS

Cell culture and GCM treatment

Microglial cultures were prepared from 1-day-old Wistar rat pups as previously described (Zawadzka & Kaminska, 2005). Briefly, cells were isolated from cerebral cortices by trypsinisation, mechanically dissociated and plated (3 × 105 cells/cm2) on poly-l-lysine-coated flasks in Dulbecco's modified Eagle medium, 4.5 g/L glucose (DMEM high glucose), with Glutamax, 10% heat-inactivated fetal bovine serum (FBS, Gibco), and antibiotics. After 10 days, microglia were collected by mild shaking and centrifugation (300 g for 5 min). Cell viability was determined by trypan blue exclusion. Cells were suspended in the culture medium, plated (2–3 × 105 cells/cm2) onto plastic Petri dishes for suspension cultures (Sarstaed) and left for 48 h before experiments. Adherent cells were >98% positive for isolectin B4. Microglia were stimulated with conditioned medium from C6 rat glioma cells (GCM). The GCM treatment was performed by replacing the medium over the microglial cells with GCM, and maintaining for 6 h, 24 h, or 48 h. The control cells were cultured for 48 h and then MGCM was pulled out and pipetted back in. The cells were cultured for further 6 h, and collected for the RNA isolation simultaneously with the 6 h point of the GCM treatment.

Glioma cells were grown in DMEM with 1 g/L glucose, 10% FBS and antibiotics. Conditioned media from glioma cells were prepared as follows: C6 cells (1 × 106) were seeded onto 100-mm dishes in a standard culture medium (DMEM low glucose) and after 24 h the medium was exchanged for 8 ml of a medium used for microglia cultures (DMEM high glucose + Glutamax). GCM was harvested after 24 h conditioning, centrifuged at 300 g for 10 min to remove cell debris, and added to microglial cultures. The design of the experiment is shown in the Fig. 1A.

RNA isolation and sequencing

Total RNA was isolated from microglial cultures with High Pure RNA kit (Roche). Quality and yield of RNAs were verified using the 2100 Bioanalyzer (Agilent Technologies) and NanoDrop 2000 (Thermo Scientific). RNA libraries for sequencing were prepared using a KAPA Stranded mRNA Sample Preparation Kit (KK8401-07962169001, Kapa Biosystems, Wilmington, MA, USA). The libraries were sequenced after onboard cluster generation using HiSeq Rapid SBS Kit v2 (200 cycles) and HiSeq PE Rapid Cluster Kit v2 (Illumina) on a HiSeq 1500 (Illumina).

Analysis of RNA-seq data

Raw sequencing data were processed using nextflow 23.04.4 and nf-core/rnaseq 3.12.0 workflow with the default options (Di Tommaso et al., 2017; Ewels et al., 2020; Patel et al., 2025). Specifically, reads quality was assessed using fastqc 0.11.9, adapters were removed with cutadapt 3.4, low quality reads were filtered out with trimgalore 0.6.7. The filtered reads were aligned to GRCr8.114 rat genome using STAR 2.7.9a, followed by quantification and mapping to genes using Salmon 1.10.1 (Dobin et al., 2013; Patro et al., 2017). BEDTools 2.30.0 and ucsc 377 were used to create bigWig coverage files. The aligned reads were sorted and indexed using samtools 1.17. Picard 3.0.0 was used to mark duplicates. RNA-seq results quality was verified using MultiQC 1.14. The Salmon-generated reads counts file (salmon.merged.gene_counts.tsv) was imported into R 4.2.3 environment, which was used for subsequent analysis and visualizations. BiomaRt 2.54.1 was used to map rows of the reads counts file to Ensembl 115 gene_biotype using ensemble_gene_id. Only the genes with the following biotypes: protein_coding, miRNA, lncRNA, were used for subsequent analysis. Differential expression analysis was performed in DESeq2 1.38.3 (Love et al., 2014). We performed the recommended variance stabilizing transformation (VST) of the DESeq2-normalized data, followed by a removal of the batch effect of the replicate number using limma 3.54.2. Neither the VST nor the batch effect removal affects the result of the DESeq2 differential expression analysis, which is not using VST data. We used the profile of every gene in DESeq2-normalized, VST- and limma-transformed data to visualize its absolute expression, and the same profile converted to Z-scores to visualize the relative changes in expression. For compactness and clarity, in the current paper we present the average expression profiles – averaged over the replicates in each group. The profiles shown are only for the genes that significantly changed expression with DESeq2 adjusted p-value for the indicated contrast(s) < 0.05. We used gprofiler2 R package, contacting the gProfiler webservice (Kolberg et al., 2020; 2023) to analyze over-representation of genes with specific functional annotations (using the mouse as the target organism because of its better annotation), namely: Reactome, KEGG and Gene Ontology, among the genes that significantly changed expression for the indicated contrasts. For visualization of the RNA-seq results aligned on the genome, BEDTools 2.30.0 and ucsc 377 were used to create bigWig coverage files for every sample. Individual loci were visualized using IGViewer 2.19.2.

In every sample, Illumina paired sequencing generated between 44 and 60 million (Samtools) of 75-76 bp (FastQC) high-quality (Phred score > 30) reads per sample, with 92% of them uniquely mapped (STAR) and, in every sample, 83-85% exonic, 11-13% intronic, 4% intergenic, with 99% of genic reads mapping to protein coding genes. Quantification of gene expression with Salmon, generated read counts for 43360 genes, all of them identified by ensembl_gene_id and gene symbol (gene_name). Using ensmaRt we mapped ensembl_gene_id to the Ensembl 115 gene symbol (external_gene_name) and the gene biotype. For further analysis we retained 20714 genes with the biotypes: protein_coding, lncRNA and miRNA that had identical symbol in the reads counts file and in Ensembl. We furthermore required a one-to-one mapping between Ensembl ensembl_gene_id and external_gene_name, which reduced the number of considered genes to 20300. The counts data for the 20300 filtered genes were analyzed for differential expression using DESeq2. As a preliminary step, after importing data into DESeq data set, we filtered out the genes with very low expression, by requiring that a gene has read counts > 10 in at least 3 (of the total of 12) samples.

Data availability

The Salmon-generated reads counts (salmon.merged.gene_counts.tsv), the results of the DESeq2 differential expression analysis (GRCr8_newComboDf.tsv), and the reads counts aligned to the genome for individual samples (bigWig), have been submitted to RepoOD (repod.icm.edu.pl) and are available at https://doi.org/10.18150/WCGKP9.

RESULTS

Time course patterns of gene expression

The RNA sequencing followed by quality filtering resulted in the dataset of 11577 genes, probed for expression under the 4 studied conditions: the MGCM-treated control group (Ctrl), and the three experimental groups treated with GCM for 6 h (H6), 24 h (H24), or 48 h (H48). The PCA plots of the top two principal components showed good reproducibility of the differences between the experimental groups within each replicate (Fig. 1B). These differences were captured by the principal component 1 (PC1), explaining 47% of the total variance. At the same time, the PCA plots also indicate a marked batch effect of the replicate number within each group. To mitigate the outcome of this batch effect on the differential expression analysis results, a paired analysis was performed, by fitting a two factor model in DESeq2, with the experimental group and the replicate number as two factors, with no interaction. In subsequent analysis the effect of the replicate number was regressed out, by analyzing contrasts between the levels of the group factor only. We also removed the batch effect of the replicate number from the VST data, which resulted in better within-the-group sample similarity and between-the-group separation in the PCA plot, facilitating its interpretation (Fig. 1C). The PCA plot in Fig. 1C demonstrates that the GCM treatment induces changes in gene expression that evolve in time, with the initial changes in expression at 6 h (H6) of the GCM treatment, as compared to the time-matched MGCM-treated control (Ctrl), reduced at 24 h (H24) of the GCM treatment and then followed by changes in the largely opposite direction at 48 h (H48) of the treatment, as indicated by the opposite sign of the change in PC1. The same conclusion can be drawn from the heatmap plot of clustered pairwise distances between the samples, shown in the Fig. 1D. The saturation of the heatmap color and the clustering dendrogram show that gene expression pattern at 6 h and at 48 h are the most different to each other, while the gene expression at 24 h is most similar, but not identical, to the MGCM control group.

In differential expression analysis, we performed two series of comparisons. In the first series of comparisons, the effect can be attributed to a single experimental factor: either the GCM treatment (H6vsCtrl), or the time following the GCM treatment (H24vsH6, H48vsH24). We used the above comparisons to describe the dynamics of the gene expression changes in response to the addition of GCM. For each gene at every comparison, we computed its log2 fold change of expression and the corresponding adjusted p-value (padj). A positive log2 fold change indicates a higher expression in the group on the left hand side of the comparison. Independently for each comparison, we identified the genes that were up-regulated (padj<0.05, log2FoldChange>0) and separately the genes that were down-regulated (padj<0.05, log2FoldChange<0), yielding a total of 6 potentially overlapping sets of genes.

To identify groups of genes with common patterns of expression, we analyzed the Venn subsets of the above 6 sets of genes. Because Venn diagrams are not well-readable for 6 sets, we show the numbers of genes in every Venn subset as a barplot (Fig. 1E). For the majority of genes marked by violet bars, their patterns of expression include a change (up or down) at the first time-point (6 h) following the GCM treatment, as compared to the time-matched control (Ctrl). Among the genes that change expression more than once, there is a clear dominance of the genes with different (up *vs.* down) directions of the changes at subsequent time points, relative to consistent directional changes. Thus, the global biphasic pattern of changes in gene expression, indicated by the PCA plot in the Fig. 1C, extends to the majority of genes that change expression at 6 h of the GCM treatment, as compared to the MGCM control.

Biphasic transcriptional response of immune genes in GCM-treated microglia

For functional interpretations of the gene expression changes, we used another series of comparisons, in which all the experimental conditions (time-points following the GCM treatment) were compared to the MGCM control (Ctrl). We performed over-representation analysis separately for each time-point, separately for the genes up-regulated (padj<0.05 and log2FoldChange>0) and down-regulated (padj<0.05 and log2FoldChange<0) at this time-point, as compared to the MGCM control. This resulted in 6 sets, each of which was independently used as input for the analysis of over-represented annotations with functional terms, from the Reactome (Jassal et al., 2020; Milacic et al., 2024), KEGG (Kanehisa et al., 2023; Kanehisa & Goto, 2000), and Gene Ontology databases (Ashburner et al., 2000; Gene Ontology Consortium et al., 2023). The inspection of the output revealed very large numbers of over-represented Gene Ontology terms, and a smaller number of terms from the Reactome and KEGG databases. The results of the over-representation analysis of terms from the Reactome and KEGG databases were represented as dot plots, permitting comparison of results between the time-points, separately for the genes up- and down-regulated at a given time-point. The presented plots show only the 10 most significantly

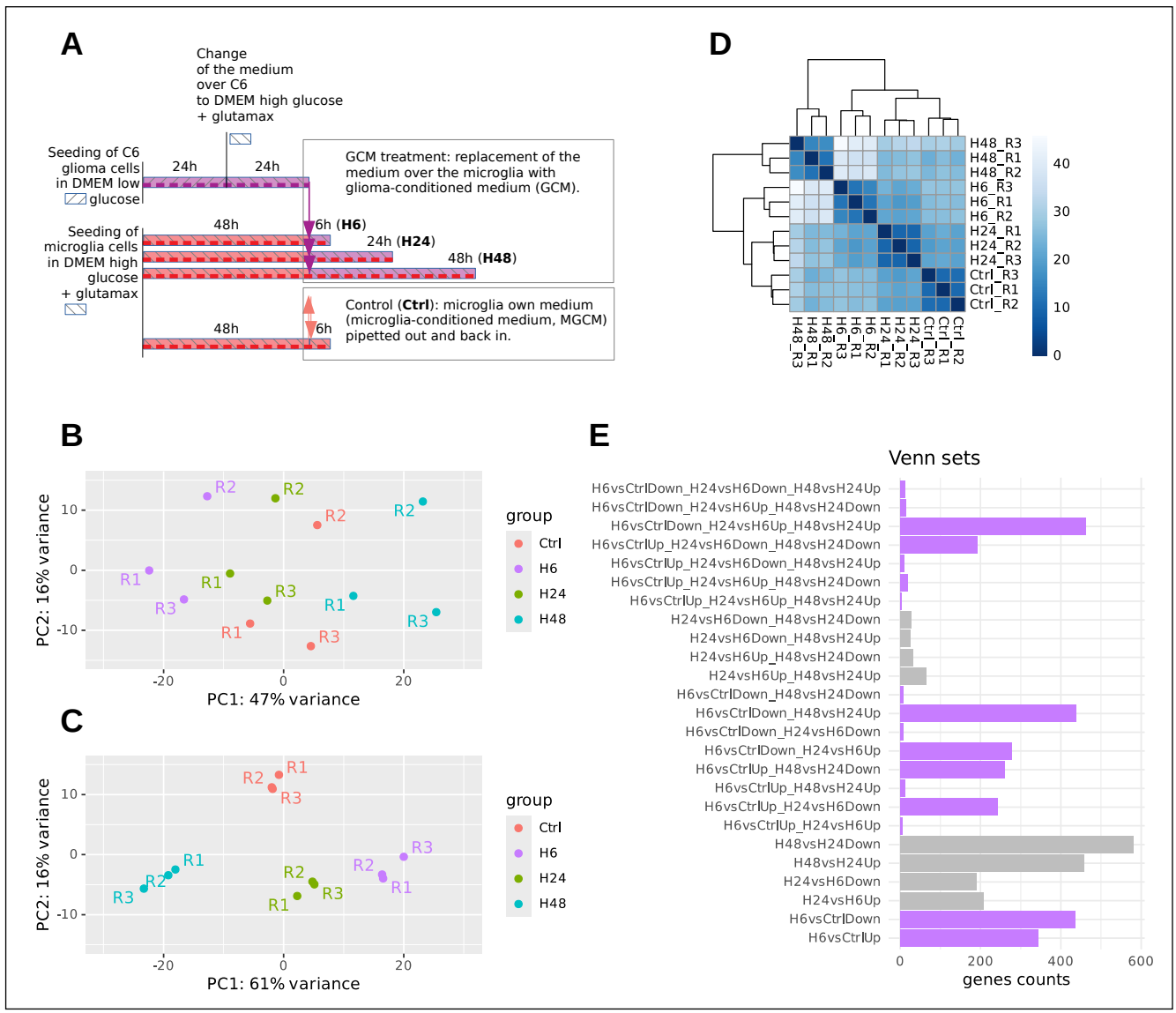

Fig. 1. Global analysis of gene expression changes induced by GCM in rat primary microglia cultures. (A) The design of the experiment. Transcriptional analysis was performed on microglia exposed to GCM for 6 h, 24 h, and 48 h, as compared to the MGCM control (Ctrl). (B, C) The results of the principal component analysis (PCA) of the DESeq2-normalized variance-stabilized (VST) data, before (B) and after the successful (C) removal of the batch effect between the biological replicates. Dots represent individual RNA samples, with the investigated groups coded by colors and labels indicate replicate numbers. (D) The heatmap of the gene expression differences between the individual samples, with the color intensity and the clustering dendrograms indicating the distance between the samples. (E) The barplot of the (nonzero) counts of genes in every Venn subset of genes with a common pattern of expression changes, among the 6 sets of the genes up-regulated (Up) or down-regulated (Down), identified separately for each of the three comparisons (H6vsCtrl, H24vsH6, H48vsH24). Up indicates higher expression at the left-hand condition of the comparison, Down – lower. The violet bars mark Venn subsets with a significant change for the H6vsCtrl comparison.

over-represented terms for each direction of change/time-point combination, sorted by decreasing significance, shown in the Fig. 2A-D.

We show the over-represented functional terms associated with gene expression down-regulation (Fig. 2A, B), and with the up-regulation (Fig. 2C, D), from the Reactome (the left column – Fig. 2A, C) and KEGG (the right column – Fig. 2B, D) databases. The time-points are represented as columns of the dot plot. At 6 h (H6vsCtrl), the two most significantly over-represented functional annotations within the down-regulated genes are: Reactome Immune System and Innate Immune System (Fig. 2A). Notably, the latter two annotations become also over-represented among the genes up-regulated at 48 h (H48vsCtrl) (Fig. 2C). The genes up-regulated at 6 h are also enriched in the KEGG anno-

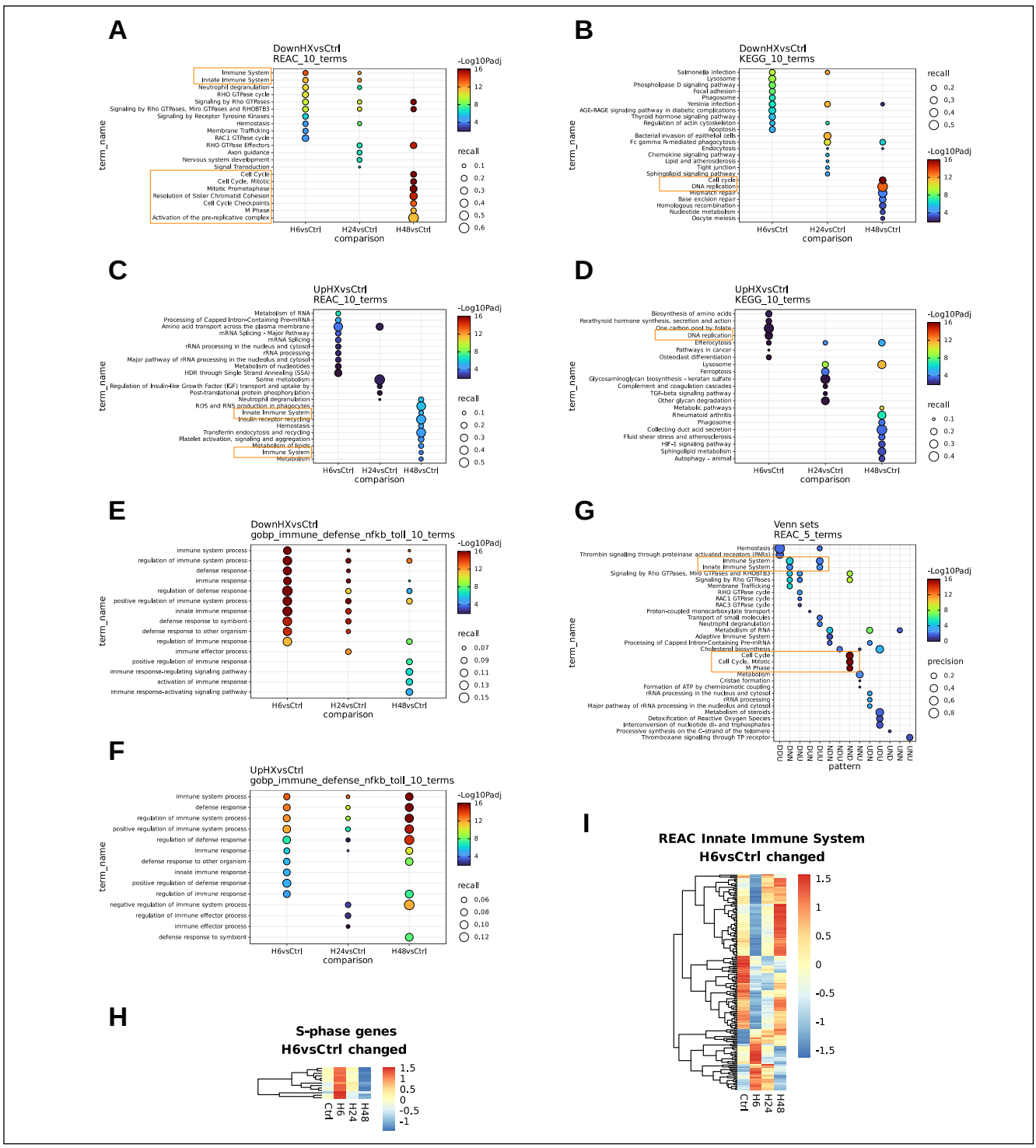

Fig. 2. Over-represented functional annotations of the genes up-regulated or down-regulated at each time-point. Transcriptional changes were compared to the MGCM control (Ctrl). The top 10 most significantly over-represented terms associated with the genes down-regulated (A, B, E), or up-regulated (C, D, F), at the indicated time-points, from the Reactome (A, C), and KEGG (B, D), and Gene Ontology (GO BP) database (E, F). In the case of Reactome and KEGG the top 10 terms were selected among all significant terms. In the case of GO BP these are the top 10 terms among a selection of significant terms – containing at least one of the phrase(s): "immune", "defense", "NF-kappaB", "toll-like" (E, F). (G) Top 5 significantly over-represented Reactome terms associated with the Venn subsets. For explanation of the abbreviated names of the Venn subsets on the X axis see the main text. Ranking on precision was used to keep the Immune System, and Innate Immune System terms in the top 5. (With the ranking on padj they would rank 4 and 10 for DNN, and 9 and 4 for DUU). (H, I) Changes in expression of S-phase specific genes from the Seurat 4.0 package (Hao et al., 2021; Tirosh et al., 2016) (H), and of the rat Reactome "Innate Immune System" genes (I), represented as average Z-scores.

tation DNA replication (Fig. 2D). The genes with several related annotations, including Cell cycle, in both Reactome and KEGG, become again over-represented among the genes down-regulated at 48 h (Fig. 2A, B). The genes annotated with immune-related Gene Ontology terms are over-represented among the genes down-regulated at 6 h and among the genes up-regulated at 48 h (Fig. 2E, F). The opposite pattern was observed for cell cycle–related genes (up-regulated at 6 h and down-regulated at 48 h) (Fig. 2B, D).

To facilitate interpretation of changes at later time-points, we performed a functional over-representation analysis of the Venn subsets (Fig. 2G). The results demonstrate that the over-representation of the cell cycle-related genes is specific to the genes in the single Venn subset H48vsH24Down, marked on the X axis as NND (which stands for: No change (H6vsCtrl), No change (H24vsH6), H48vsH24Down). These genes change their expression for the first time at 48 h of culture. Conversely, the genes with immune-related Reactome annotations: Immune System, and Innate Immune System; are over-represented among the genes in the Venn subsets: H6vsCtrlDown (DNN), and H6vsCtrlDown_H24vsH6Up_H48vsH24Up (DUU). The expression profiles of these genes are affected by the GCM treatment, because they begin with down-regulation in response to GCM. This down-regulation is either persistent (DNN), or followed by up-regulation (DUU).

The expression of S phase-associated genes regulated at 6 h by GCM, as compared to the MGCM control, is illustrated in the heatmap shown in the Fig. 2H. A visualization of expression profiles of the Reactome Innate Immune System genes (Fig. 2I) shows that under the condition of the GCM treatment the changes in expression of multiple immune-related genes are biphasic, with initial down-regulation, followed by up-regulation to the level comparable or higher than observed in the control cells (Ctrl). There are, however, Reactome Innate Immune System genes that become up-regulated at 6 h and remain up-regulated at 48 h (Fig. 3A). Conversely, there are also Reactome Innate Immune System genes down-regulated at 6 h that remain down-regulated at 48 h. The persistently down-regulated genes include *Tlr9* and *Myd8*, marked by rectangles in Fig. 3B.

In addition, we also looked at changes in expression in categories of genes that we considered as relevant for the microglia response to glioma, including the genes encoding: interleukins and chemokines and their receptors, *Tnf* family and *Tgfb* family ligands and receptors. The expression profiles of the genes in these categories that significantly changed expression at 6 h of the GCM treatment, as compared to the time matched MGCM control (Ctrl), are shown in the Fig. 3C-F. In these categories multiple genes, mostly encoding interleukins, become transiently up-regulated at 6 h and then down-regulated. This group includes *Il7*, *Il18*, *Il4r*, *Il6r* (Fig. 3C), and *Tgfbrap1* (Fig. 3F). Another group, including *Il1rn*, *Il33* (Fig. 3C), and *Ccr1*, *Ccl22* (Fig. 3D), only became up-regulated at 48 h. Notably, *Il1a*, *Cxcl16,* and *Tgfbr1,2* (marked by rectangles) become up-regulated at 6 h and remain up-regulated at later time-points. Furthermore, *Cxcl16* was expressed at a high absolute level (DESeq2 normalized counts about 7000). The data on absolute expression are available in the RepOD, in the file GRCr8_newComboDf_v5.tab, at https://doi.org/10.18150/WCGKP9. *Tgfb1* becomes down-regulated at 6-24 h and then up-regulated above the MGCM control level at 48 h. Conversely, *Il1b* (Fig. 3C) becomes down-regulated at 6 h and remains down-regulated at 48 h.

Microglial gene expression changes during prolonged culture in GCM

The early down-regulation of many immune-related genes and their later up-regulation prompted us to compare the changes in expression in the current RNA-seq experiment with the results of the earlier microarray study, in which we characterized the changes at 6 h following treatment with GCM or 100 ng/ml LPS, as compared to the 6 h MGCM control (Ellert-Miklaszewska et al., 2013). We calculated Pearson's correlation coefficients between the log2 fold changes, thereafter referred to as "changes", of expression for indicated comparisons for the genes that showed significant change in expression in both experiments (Fig. 3G, H). As expected, the changes at 6 h of GCM treatment in the current study (H6vsCtrl) and in the previous microarray study (GCMvsCTRL) show good correlation. The changes between the later consecutive time-points (H24vsH6 and H48vsH24) were anti-correlated with the changes at 6 h of the GCM treatment, as compared to the 6 h MGCM control (H6vsCtrl). Despite this, the changes at the two later time points, as compared to the control (H24vsCtrl and H48vsCtrl) showed positive correlations with the changes at 6 h (H6vsCtrl), demonstrating that the initial changes in response to the GCM were stronger then subsequent changes in the opposite direction. Comparison of the GCM-induced changes in the current study with the changes at 6 h after the addition of LPS (Fig. 3H), showed that the changes induced at 6 h by GCM were negatively correlated with the changes following LPS, whereas the changes at 48 h GCM (H48vsH24 and H48vsCtrl) were positively correlated with the changes at 6 h of LPS (LPSvsCTRL).

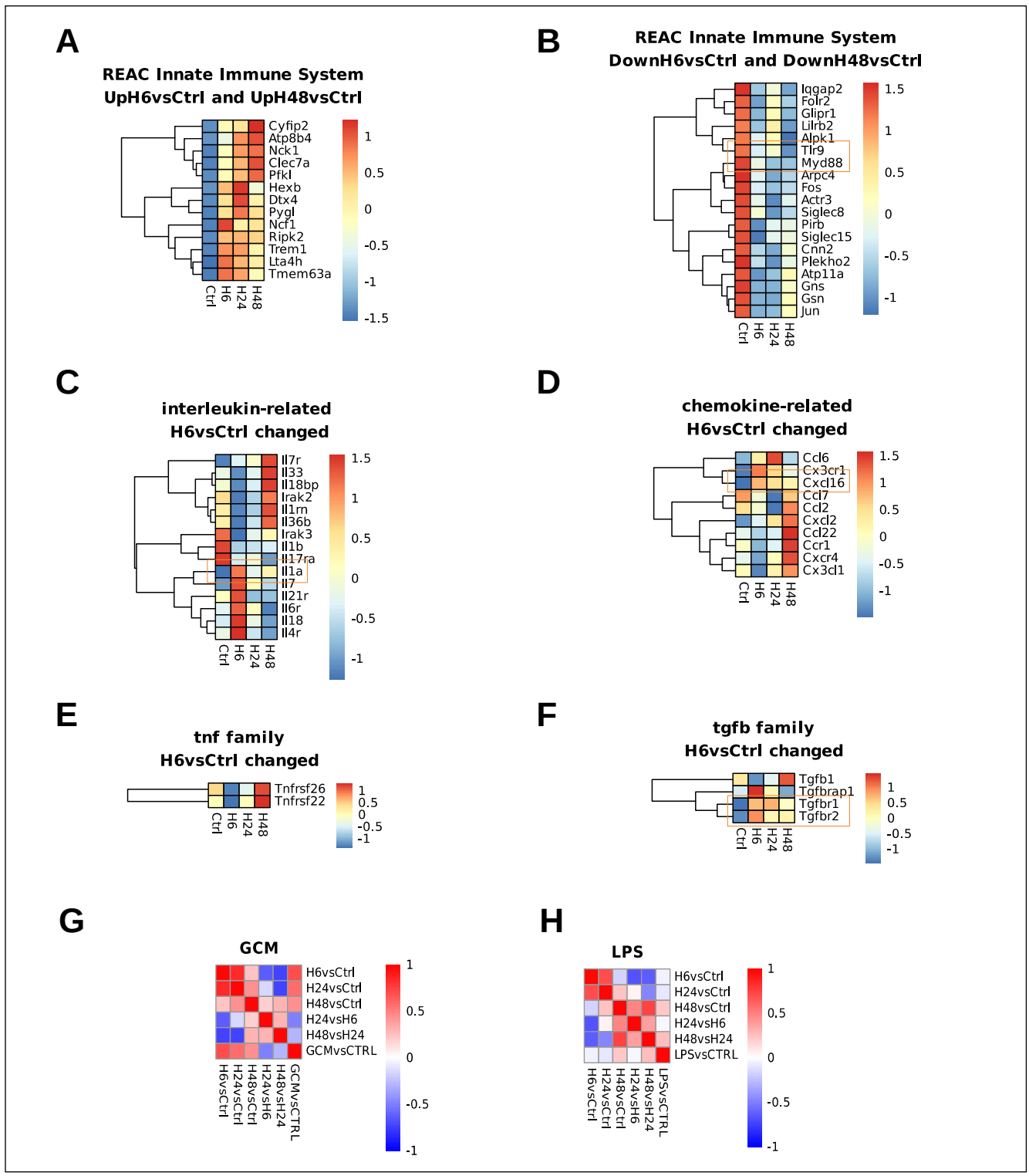

Fig. 3. Gene expression profiles of selected groups of genes, for the genes that significantly changed expression at 6 h of the GCM treatment, as compared to the 6 h MGCM control. (A, B) Heatmaps of the changes in gene expression, represented as average Z-scores, for the rat Reactome "Innate Immune System" genes persistently up-regulated (A), or persistently down-regulated (B) by the GCM treatment. Heatmaps of the changes in gene expression for interleukin-related genes (C), chemokines and their receptors (D), *Tnf* family genes (E), and *Tgfb* family genes (F). Global correlations of gene expression changes in the current experiment with published microarray data on the changes induced at the 6 h time-point by GCM or LPS (G, H), shown as Pearson correlation coefficients between the log2 fold changes in either experiment, for the genes that in both experiments significantly changed expression at 6 h of the GCM treatment, or at 6 h LPS treatment, as compared to the 6 h MGCM control.

Induction of thromboxane synthesis genes in microglial response to GCM

To identify novel genes potentially involved in the early microglial response to GCM, we focused at changes occurring at 6 h. The expression changes at this time-point, relative to the time-matched MGCM control (Ctrl), are presented as a volcano plot in the Fig. 4A. The 40 most significantly regulated genes (those with the largest –log10 adjusted p-values) are labeled. Among these are several genes previously reported as up-regulated in microglia exposed to glioma, including *Smad7* and MHC class II components (*RT1-DMa*, *RT1-DMb*), as well as established microglial markers *Cx3cr1* and *Tmem119*. Among the most induced transcripts, *Ptgs1* (also known as *Cox1*) and *Tbxas1* stood out because they encode two enzymes – prostaglandin-endoperoxide synthase 1 and thromboxane A synthase 1 – responsible for the conversion of arachidonic acid to thromboxane A2 (TXA2), a potent lipid mediator that can modulate inflammatory signaling and microglial activation (Fig. 4B). The RNA-seq read coverage data confirmed high expression levels, strong reproducibility across biological replicates, and robust induction of both genes by the GCM treatment (Fig. 4C, D).

DISCUSSION

Microglia that accumulate in malignant gliomas exhibit the immunosuppressive phenotype. Our previous studies revealed a list of genes upregulated in microglia early (6 h) in response to the stimulation with GCM. However, these genes are not upregulated in microglia isolated from gliomas (typically tested at 7 or 14, 21 days after glioma cell implantation), suggesting their transient activation. In this study, we aimed to identify genes that are activated and remain upregulated following glioma stimulation.

We found the dominant biphasic pattern of gene expression changes following the exposure to the GCM, which was unexpected. Our results reveal that most gene expression changes observed at 6 hours are transient. At the subsequent time-points, the transcriptional profile shifts toward a state more closely resembling that of microglia 6 hours after LPS stimulation than the one observed 6 hours after GCM.

This swing-like pattern of the changes in expression of a majority of genes following the GCM treatment may be a consequence of its single addition. It is likely that the factors present in the GCM become used-up or degraded at the later time-points during the cell culture progression. Additionally, the late down-regulation of the S-phase genes might be related to using-up the nutrients or inhibition of cell division due to an increased cell density.

Ideally, time-matched MGCM controls for every time-point of the GCM treatment should be employed. However, a number of primary microglia cells that can be obtained from a single microglia preparation is limiting, and we chose the experiment design with three time-points following the GCM treatment, and the MGCM control only for the earliest (6 h) time-point. We reasoned that if a gene changes expression in response to GCM at the earliest time-point of the treatment the latter evolution of its expression will also be affected. This assumption is corroborated by changes in the chromatin structure induced by the GCM treatment observed in our previous work (Przanowski et al., 2019; Maleszewska et al., 2021).

Alternatively, the biphasic response may reflect the *in vivo* dynamics of the response to the factors secreted by glioma. We had previously identified Spp1 as one of such factors, and showed that its distinct cleavage forms have different effects on microglia (Ellert-Miklaszewska et al., 2016). This second possibility is supported by the fact that some of the genes up-regulated at 48 h, such as *Il1rn*, *Ccl2*, *Ccl22*, and *Cxcl16*, are also up-regulated in the glioma *in vivo* (Gieryng et al., 2017a). *Ccl2*, which is also produced by glioma (Takacs et al., 2022), is involved in regulation of oriented migration and penetrative infiltration of tumor mainly by monocytes/macrophages (reviewed in Vakilian et al., 2017). The comparison of the current *in vitro* data with our earlier *in vivo* data is complicated by different timing (48 hours after GCM *in vitro vs.* 21 days after glioma implantation *in vivo*).

We focus on the genes annotated in the Reactome database to the innate immune system, and the 40 genes that were most significantly regulated in either direction at 6 h. This filtering has resulted in identification of at least 13 innate immune response genes that were stably up-regulated by the GCM treatment. Notably, these genes include genes encoding key molecules involved in signaling, such as: Trem1 – a marker of GAMs (Ispirjan et al., 2024) and prognostic indicator in glioma (Dong et al., 2024; Zhang et al., 2024); Clec7a – expressed on glioma-associated M2 macrophages (Wang et al., 2024); Ripk2 (alias Rip2) – inducing temozolomide resistance and PD-L1 up-regulation when overexpressed in GBM cells (Liu et al., 2025); Lta4h – a LTB4 synthase (Li et al., 2021); as well as metabolic genes, including: *Hexb* – involved in microglia-neuron (Frosch et al., 2025) and TAM-GBM (Zhu et al., 2024) metabolic cross-talk; *Pygl* – encoding glycogen phosphorylase (Abbadi et al., 2014), *Ncf1* – encoding a NADPH oxidase subunit (Ding et al., 2017); *Pfkl* – encoding the core rate-limiting enzyme of glycolysis important in cancer – reviewed in

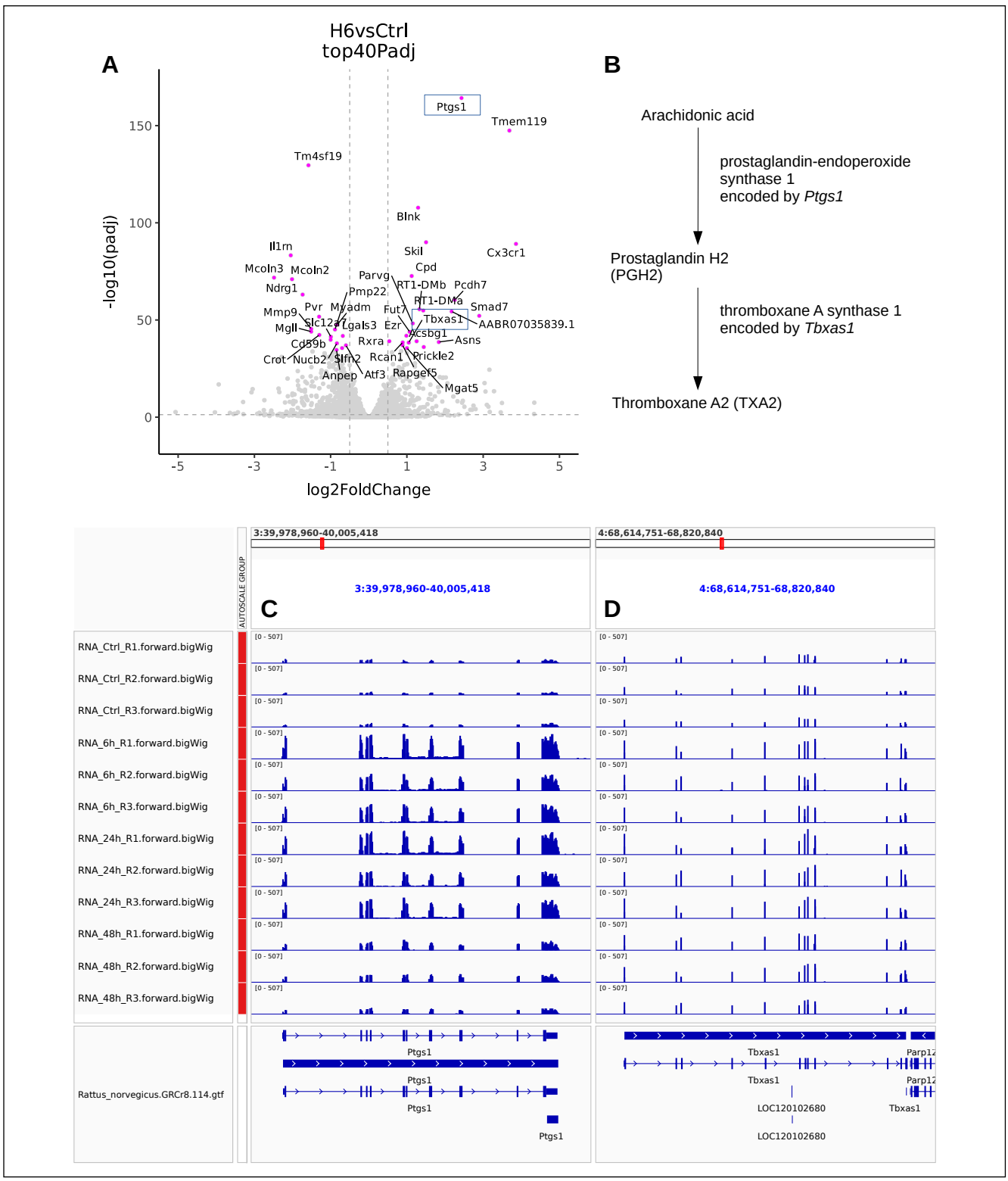

Fig. 4. Unbiased identification of the genes most significantly regulated in the thromboxane A2 synthesis pathway. The gene expression at 6 h of the GCM treatment is shown and the row reads counts aligned to the genome for the two genes. (A) A volcano plot of the changes in gene expression at 6 h after GCM, as compared to the time-matched MGCM control (Ctrl). The dots representing the top 40 most significantly regulated genes are indicated by color (magenta) as well as labeled with the gene symbols. The two genes encoding enzymes in the thromboxane A2 (TXA2) biosynthesis pathway are indicated by rectangles. (B) Thromboxane A2 biosynthesis pathway. (C, D) The reads counts aligned to the genome for individual RNA samples in the loci of *Ptgs1* (C) and *Tbxas1* (D).

(Yuan et al., 2025). A larger number of 19 innate immune response genes were stably down-regulated by the GCM treatment, and these genes notably include *Tlr9* and *Myd88*. Tlr9 is an endosomal membrane-bound protein that binds to CpG-containing microbial DNA or endogenous signals from dead cells or tissue damage. Inhibition of Tlr9-Myd88 interaction blocks Tlr9-mediated gene induction (Veleeparambil et al., 2025). In GBM cells Tlr9 is important for Stat3 activation (Hung et al., 2025) and induction of *Mmp2,9,13* in glioma cells (reviewed in Fehri et al., 2022), and of *Mmp9* in microglia and macrophages (Tiwari et al., 2021). Glioma-released factors trigger the expression and activity of Mmp14 via microglial toll-like receptors and the p38 MAPK pathway, as deletion of the toll-like receptor adapter protein Myd88 or p38 inhibition prevented Mmp14 expression and activity in cultured microglial cells. Microglial Mmp14 then activates glioma-derived pro-Mmp2 and promotes glioma expansion (Markovic et al., 2009). In addition to innate immune genes, we looked into changes in cytokines, chemokines and related genes. Among them, *Cxcl16*, and *Tgfbr1* and *Tgfbr2* were early stably up-regulated at 6 h and at 48 h. *Cxcl16* encodes a chemokine that drive microglia polarization towards an anti-inflammatory phenotype (Lepore et al., 2018). *Tgfb1* was transiently down-regulated at 6 h and subsequently up-regulated at 48 h showing a pattern opposite to that of the S-phase genes, consistent with known ability of *Tgfb1* to inhibit microglia proliferation (Jones et al., 1998).

Among the top 40 most significantly affected genes, we identified *Ptgs1* (alias *Cox1*) and *Tbxas1*, encoding the two enzymes in the TXA2 biosynthesis pathway (Fig. 4B). *Ptgs1* encodes prostaglandin-endoperoxide synthase 1, which catalyzes the conversion of arachidonic acid into prostaglandin H2. *Tbxas1* encodes thromboxane A synthase 1, which catalyzes the conversion of prostaglandin H2 to thromboxane A2 (Ashton et al., 2022). These finding are particularly interesting in the context of several recent studies related to cancer, including glioma. Inhibitors of cyclooxygenase 1 (COX-1), including aspirin, enhance immune response to cancer metastasis, by releasing T cells from suppression by platelet-derived TXA2 (Yang et al., 2025). The COX-1 protein is elevated in both low and high grade gliomas, including glioblastoma, where it is expressed in a subset of macrophages/microglia cells and not in the tumor cells (Deininger et al., 1999). The up-regulation of *Ptgs1* and *Tbxas1* in rat microglia cells in response to factors from C6 glioma raises the possibility of increased TXA2 synthesis, which may contribute to the T cell immunosuppression observed in glioma tumors and could be targeted with commonly used drugs. Testing this possibility requires further studies. Before embarking on such studies, a word of caution is needed: while our transcriptomic evidence on the early and persistent induction of both genes is strong, a major limitation of the current study is the lack of the confirmation of these findings at the protein expression or at the TXA2 synthesis level.

CONCLUSIONS

Changes induced by GCM treatment are transient for the majority of genes, but stable changes that last up to 48 h were observed for some of the key genes.

Changes observed at 6 h of GCM treatment are consistent with previous published microarray findings, but extend for additional genes.

Most notably, among the genes induced at 6 h by the GCM treatment that remain up-regulated for 48 h are those encoding the enzymes involved in the synthesis of thromboxane A2, which is known to induce T cell suppression.

ACKNOWLEDGMENTS

The study was supported by European Regional Development Fund, Foundation for Polish Science. Grant Number: HOMING PLUS/2011-3/7 (MM).

REFERENCES

Abbadi, S., Rodarte, J. J., Abutaleb, A., Lavell, E., Smith, C. L., Ruff, W., Schiller, J., Olivi, A., Levchenko, A., Guerrero-Cazares, H., & Quinones-Hinojosa, A. (2014). Glucose-6-phosphatase is a key metabolic regulator of glioblastoma invasion. *Molecular Cancer Research: MCR*, *12*(11), 1547–1559. https://doi.org/10.1158/1541-7786.MCR-14-0106-T

Ashburner, M., Ball, C. A., Blake, J. A., Botstein, D., Butler, H., Cherry, J. M., Davis, A. P., Dolinski, K., Dwight, S. S., Eppig, J. T., Harris, M. A., Hill, D. P., Issel-Tarver, L., Kasarskis, A., Lewis, S., Matese, J. C., Richardson, J. E., Ringwald, M., Rubin, G. M., & Sherlock, G. (2000). Gene ontology: Tool for the unification of biology. The Gene Ontology Consortium. *Nature Genetics*, *25*(1), 25–29. https://doi.org/10.1038/75556

Ashton, A. W., Zhang, Y., Cazzolli, R., & Honn, K. V. (2022). The Role and Regulation of Thromboxane A2 Signaling in Cancer-Trojan Horses and Misdirection. *Molecules (Basel, Switzerland)*, *27*(19), 6234. https://doi.org/10.3390/molecules27196234

Bowman, R. L., Klemm, F., Akkari, L., Pyonteck, S. M., Sevenich, L., Quail, D. F., Dhara, S., Simpson, K., Gardner, E. E., Iacobuzio-Donahue, C. A., Brennan, C. W., Tabar, V., Gutin, P. H., & Joyce, J. A. (2016). Macrophage Ontogeny Underlies Differences in Tumor-Specific Education in Brain Malignancies. *Cell Reports*, *17*(9), 2445–2459. https://doi.org/10.1016/j.celrep.2016.10.052

Buonfiglioli, A., & Hambardzumyan, D. (2021). Macrophages and microglia: The cerberus of glioblastoma. *Acta Neuropathologica Communications*, *9*(1), 54. https://doi.org/10.1186/s40478-021-01156-z

Butovsky, O., Jedrychowski, M. P., Moore, C. S., Cialic, R., Lanser, A. J., Gabriely, G., Koeglsperger, T., Dake, B., Wu, P. M., Doykan, C. E., Fanek, Z.,

Liu, L., Chen, Z., Rothstein, J. D., Ransohoff, R. M., Gygi, S. P., Antel, J. P., & Weiner, H. L. (2014). Identification of a unique TGF-β-dependent molecular and functional signature in microglia. *Nature Neuroscience*, *17*(1), 131–143. https://doi.org/10.1038/nn.3599

Deininger, M. H., Weller, M., Streffer, J., Mittelbronn, M., & Meyermann, R. (1999). Patterns of cyclooxygenase-1 and -2 expression in human gliomas in vivo. *Acta Neuropathologica*, *98*(3), 240–244. https://doi.org/10.1007/s004010051075

Di Tommaso, P., Chatzou, M., Floden, E. W., Barja, P. P., Palumbo, E., & Notredame, C. (2017). Nextflow enables reproducible computational workflows. *Nature Biotechnology*, *35*(4), 316–319. https://doi.org/10.1038/nbt.3820

Ding, X., Zhang, M., Gu, R., Xu, G., & Wu, H. (2017). Activated microglia induce the production of reactive oxygen species and promote apoptosis of co-cultured retinal microvascular pericytes. *Graefe's Archive for Clinical and Experimental Ophthalmology*, *255*(4), 777–788. https://doi.org/10.1007/s00417-016-3578-5

Dobin, A., Davis, C. A., Schlesinger, F., Drenkow, J., Zaleski, C., Jha, S., Batut, P., Chaisson, M., & Gingeras, T. R. (2013). STAR: Ultrafast universal RNA-seq aligner. *Bioinformatics (Oxford, England)*, *29*(1), 15–21. https://doi.org/10.1093/bioinformatics/bts635

Dong, M., Zhang, X., Peng, P., Chen, Z., Zhang, Y., Wan, L., Xiang, W., Liu, G., Guo, Y., Xiao, Q., Wang, B., Guo, D., Zhu, M., Yu, X., & Wan, F. (2024). Hypoxia-induced TREM1 promotes mesenchymal-like states of glioma stem cells via alternatively activating tumor-associated macrophages. *Cancer Letters*, *590*, 216801. https://doi.org/10.1016/j.canlet.2024.216801

Ellert-Miklaszewska, A., Dabrowski, M., Lipko, M., Sliwa, M., Maleszewska, M., & Kaminska, B. (2013). Molecular definition of the pro-tumorigenic phenotype of glioma-activated microglia. *Glia*, *61*(7), 1178–1190. https://doi.org/10.1002/glia.22510

Ellert-Miklaszewska, A., Wisniewski, P., Kijewska, M., Gajdanowicz, P., Pszczolkowska, D., Przanowski, P., Dabrowski, M., Maleszewska, M., & Kaminska, B. (2016). Tumour-processed osteopontin and lactadherin drive the protumorigenic reprogramming of microglia and glioma progression. *Oncogene*, *35*(50), 6366–6377. https://doi.org/10.1038/onc.2016.55

Ewels, P. A., Peltzer, A., Fillinger, S., Patel, H., Alneberg, J., Wilm, A., Garcia, M. U., Di Tommaso, P., & Nahnsen, S. (2020). The nf-core framework for community-curated bioinformatics pipelines. *Nature Biotechnology*, *38*(3), 276–278. https://doi.org/10.1038/s41587-020-0439-x

Fehri, E., Ennaifer, E., Bel Haj Rhouma, R., Ardhaoui, M., & Boubaker, S. (2022). TLR9 and Glioma: Friends or Foes? *Cells*, *12*(1), 152. https://doi.org/10.3390/cells12010152

Frosch, M., Shimizu, T., Wogram, E., Amann, L., Gruber, L., Groisman, A. I., Fliegauf, M., Schwabenland, M., Chhatbar, C., Zechel, S., Rosewich, H., Gärtner, J., Quintana, F. J., Buescher, J. M., Blank, T., Binder, H., Stadelmann, C., Letzkus, J. J., Hopf, C., … Prinz, M. (2025). Microglia-neuron crosstalk through Hex-GM2-MGL2 maintains brain homeostasis. *Nature*, *646*(8086), 913–924. https://doi.org/10.1038/s41586-025-09477-y

Gabrusiewicz, K., Ellert-Miklaszewska, A., Lipko, M., Sielska, M., Frankowska, M., & Kaminska, B. (2011). Characteristics of the alternative phenotype of microglia/macrophages and its modulation in experimental gliomas. *PloS One*, *6*(8), e23902. https://doi.org/10.1371/journal.pone.0023902

Gene Ontology Consortium, Aleksander, S. A., Balhoff, J., Carbon, S., Cherry, J. M., Drabkin, H. J., Ebert, D., Feuermann, M., Gaudet, P., Harris, N. L., Hill, D. P., Lee, R., Mi, H., Moxon, S., Mungall, C. J., Muruganugan, A., Mushayahama, T., Sternberg, P. W., Thomas, P. D., … Westerfield, M. (2023). The Gene Ontology knowledgebase in 2023. *Genetics*, *224*(1), iyad031. https://doi.org/10.1093/genetics/iyad031

Gieryng, A., Pszczolkowska, D., Bocian, K., Dabrowski, M., Rajan, W. D., Kloss, M., Mieczkowski, J., & Kaminska, B. (2017a). Immune microenvironment of experimental rat C6 gliomas resembles human glioblastomas. *Scientific Reports*, *7*(1), 17556. https://doi.org/10.1038/s41598-017-17752-w

Gieryng, A., Pszczolkowska, D., Walentynowicz, K. A., Rajan, W. D., & Kaminska, B. (2017b). Immune microenvironment of gliomas. *Laboratory Investigation; a Journal of Technical Methods and Pathology*, *97*(5), 498–518. https://doi.org/10.1038/labinvest.2017.19

Hao, Y., Hao, S., Andersen-Nissen, E., Mauck, W. M., Zheng, S., Butler, A., Lee, M. J., Wilk, A. J., Darby, C., Zager, M., Hoffman, P., Stoeckius, M., Papalexi, E., Mimitou, E. P., Jain, J., Srivastava, A., Stuart, T., Fleming, L. M., Yeung, B., … Satija, R. (2021). Integrated analysis of multimodal single-cell data. *Cell*, *184*(13), 3573–3587.e29. https://doi.org/10.1016/j.cell.2021.04.048

Hung, C. Y., Kang, E. Y., Jacek, K., Yu, C., Zhang, X., Zhu, Y., Aftabizadeh, M., Wong, R. A., Badie, B., Świderski, P., Kamińska, B., Alizadeh, D., Heimberger, A. B., Brown, C. E., & Kortylewski, M. (2025). Multimodal glioma immunotherapy combining TLR9-targeted STAT3 antisense oligodeoxynucleotides with PD1 immune checkpoint blockade. *Neuro-Oncology*, *27*(9), 2296–2312. https://doi.org/10.1093/neuonc/noaf099

Ispirjan, M., Marx, S., Freund, E., Fleck, S. K., Baldauf, J., Roessler, K., Schroeder, H. W. S., & Bekeschus, S. (2024). Markers of tumor-associated macrophages and microglia exhibit high intratumoral heterogeneity in human glioblastoma tissue. *Oncoimmunology*, *13*(1), 2425124. https://doi.org/10.1080/2162402X.2024.2425124

Jassal, B., Matthews, L., Viteri, G., Gong, C., Lorente, P., Fabregat, A., Sidiropoulos, K., Cook, J., Gillespie, M., Haw, R., Loney, F., May, B., Milacic, M., Rothfels, K., Sevilla, C., Shamovsky, V., Shorser, S., Varusai, T., Weiser, J., … D'Eustachio, P. (2020). The reactome pathway knowledgebase. *Nucleic Acids Research*, *48*(D1), D498–D503. https://doi.org/10.1093/nar/gkz1031

Jones, L. L., Kreutzberg, G. W., & Raivich, G. (1998). Transforming growth factor beta's 1, 2 and 3 inhibit proliferation of ramified microglia on an astrocyte monolayer. *Brain Research*, *795*(1–2), 301–306. https://doi.org/10.1016/s0006-8993(98)00325-4

Kanehisa, M., Furumichi, M., Sato, Y., Kawashima, M., & Ishiguro-Watanabe, M. (2023). KEGG for taxonomy-based analysis of pathways and genomes. *Nucleic Acids Research*, *51*(D1), D587–D592. https://doi.org/10.1093/nar/gkac963

Kanehisa, M., & Goto, S. (2000). KEGG: Kyoto encyclopedia of genes and genomes. *Nucleic Acids Research*, *28*(1), 27–30. https://doi.org/10.1093/nar/28.1.27

Kirschenbaum, D., Xie, K., Ingelfinger, F., Katzenelenbogen, Y., Abadie, K., Look, T., Sheban, F., Phan, T. S., Li, B., Zwicky, P., Yofe, I., David, E., Mazuz, K., Hou, J., Chen, Y., Shaim, H., Shanley, M., Becker, S., Qian, J., … Amit, I. (2024). Time-resolved single-cell transcriptomics defines immune trajectories in glioblastoma. *Cell*, *187*(1), 149–165.e23. https://doi.org/10.1016/j.cell.2023.11.032

Kolberg, L., Raudvere, U., Kuzmin, I., Adler, P., Vilo, J., & Peterson, H. (2023). G: Profiler-interoperable web service for functional enrichment analysis and gene identifier mapping (2023 update). *Nucleic Acids Research*, *51*(W1), W207–W212. https://doi.org/10.1093/nar/gkad347

Kolberg, L., Raudvere, U., Kuzmin, I., Vilo, J., & Peterson, H. (2020). gprofiler2—An R package for gene list functional enrichment analysis and namespace conversion toolset g: Profiler. *F1000Research*, *9*, ELIXIR-709. https://doi.org/10.12688/f1000research.24956.2

Lepore, F., D'Alessandro, G., Antonangeli, F., Santoro, A., Esposito, V., Limatola, C., & Trettel, F. (2018). CXCL16/CXCR6 Axis Drives Microglia/Macrophages Phenotype in Physiological Conditions and Plays a Crucial Role in Glioma. *Frontiers in Immunology*, *9*, 2750. https://doi.org/10.3389/fimmu.2018.02750

Li, H., Wang, Y., Wang, B., Li, M., Liu, J., Yang, H., & Shi, Y. (2021). Baicalin and Geniposide Inhibit Polarization and Inflammatory Injury of OGD/R-Treated Microglia by Suppressing the 5-LOX/LTB4 Pathway. *Neurochemical Research*, *46*(7), 1844–1858. https://doi.org/10.1007/s11064-021-03305-1

Liu, Xiaomeng, Liu, Xiaosong, Zhao, L., Wu, J., Wang, X., & Hu, Y. (2025). RIP2/NF-κB/PD-L1 signaling pathway is involved in temozolomide resistance by inducing autophagy in glioblastoma cells. *Translational Oncology*, *58*, 102424. https://doi.org/10.1016/j.tranon.2025.102424

Love, M. I., Huber, W., & Anders, S. (2014). Moderated estimation of fold change and dispersion for RNA-seq data with DESeq2. *Genome Biology*, *15*(12), 550. https://doi.org/10.1186/s13059-014-0550-8

Maleszewska, M., Steranka, A., Smiech, M., Kaza, B., Pilanc, P., Dabrowski, M., & Kaminska, B. (2021). Sequential changes in histone modifications shape transcriptional responses underlying microglia polarization by glioma. *Glia*, *69*(1), 109–123. https://doi.org/10.1002/glia.23887

Markovic, D. S., Vinnakota, K., Chirasani, S., Synowitz, M., Raguet, H., Stock, K., Sliwa, M., Lehmann, S., Kälin, R., van Rooijen, N., Holmbeck, K., Heppner, F. L., Kiwit, J., Matyash, V., Lehnardt, S., Kaminska, B., Glass, R., & Kettenmann, H. (2009). Gliomas induce and exploit microglial MT1-MMP expression for tumor expansion. *Proceedings of the National Academy of Sciences of the United States of America*, *106*(30), 12530–12535. https://doi.org/10.1073/pnas.0804273106

Milacic, M., Beavers, D., Conley, P., Gong, C., Gillespie, M., Griss, J., Haw, R., Jassal, B., Matthews, L., May, B., Petryszak, R., Ragueneau, E., Rothfels, K., Sevilla, C., Shamovsky, V., Stephan, R., Tiwari, K., Varusai, T., Weiser, J., … D'Eustachio, P. (2024). The Reactome Pathway Knowledgebase 2024. *Nucleic Acids Research*, *52*(D1), D672–D678. https://doi.org/10.1093/nar/gkad1025

Ochocka, N., Segit, P., Walentynowicz, K. A., Wojnicki, K., Cyranowski, S., Swatler, J., Mieczkowski, J., & Kaminska, B. (2021). Single-cell RNA sequencing reveals functional heterogeneity of glioma-associated brain macrophages. *Nature Communications*, *12*(1), 1151. https://doi.org/10.1038/s41467-021-21407-w

Ochocka, N., Segit, P., Wojnicki, K., Cyranowski, S., Swatler, J., Jacek, K., Grajkowska, W., & Kaminska, B. (2023). Specialized functions and sexual dimorphism explain the functional diversity of the myeloid populations during glioma progression. *Cell Reports*, *42*(1), 111971. https://doi.org/10.1016/j.celrep.2022.111971

Patel, H., Manning, J., Ewels, P., Garcia, M. U., Peltzer, A., Hammarén, R., Botvinnik, O., Talbot, A., Hanssen, F., Sturm, G., bot, nf-core, Zepper, M., Moreno, D., Vemuri, P., Binzer-Panchal, M., Greenberg, E., silviamorins, Pantano, L., Syme, R., … Zhou, P. (2025). *nf-core/rnaseq: Nf-core/rnaseq v3.21.0 – Mercury Macaw* [Computer software]. Zenodo. https://doi.org/10.5281/zenodo.17153746

Patro, R., Duggal, G., Love, M. I., Irizarry, R. A., & Kingsford, C. (2017). Salmon provides fast and bias-aware quantification of transcript expression. *Nature Methods*, *14*(4), 417–419. https://doi.org/10.1038/nmeth.4197

Pombo Antunes, A. R., Scheyltjens, I., Lodi, F., Messiaen, J., Antoranz, A., Duerinck, J., Kancheva, D., Martens, L., De Vlaminck, K., Van Hove, H., Kjølner Hansen, S. S., Bosisio, F. M., Van der Borght, K., De Vleeschouwer, S., Sciot, R., Bouwens, L., Verfaillie, M., Vandamme, N., Vandenbroucke, R. E., … Movahedi, K. (2021). Single-cell profiling of myeloid cells in glioblastoma across species and disease stage reveals macrophage competition and specialization. *Nature Neuroscience*, *24*(4), 595–610. https://doi.org/10.1038/s41593-020-00789-y

Prinz, M., Tay, T. L., Wolf, Y., & Jung, S. (2014). Microglia: Unique and common features with other tissue macrophages. *Acta Neuropathologica*, *128*(3), 319–331. https://doi.org/10.1007/s00401-014-1267-1

Przanowski, P., Mondal, S. S., Cabaj, A., Dębski, K. J., Wojtas, B., Gielniewski, B., Kaza, B., Kaminska, B., & Dabrowski, M. (2019). Open chromatin landscape of rat microglia upon proinvasive or inflammatory polarization. *Glia*, *67*(12), 2312–2328. https://doi.org/10.1002/glia.23686

Roura, A.-J., Gielniewski, B., Pilanc, P., Szadkowska, P., Maleszewska, M., Krol, S. K., Czepko, R., Kaspera, W., Wojtas, B., & Kaminska, B. (2021). Identification of the immune gene expression signature associated with recurrence of high-grade gliomas. *Journal of Molecular Medicine (Berlin, Germany)*, *99*(2), 241–255. https://doi.org/10.1007/s00109-020-02005-7

Sielska, M., Przanowski, P., Wylot, B., Gabrusiewicz, K., Maleszewska, M., Kijewska, M., Zawadzka, M., Kucharska, J., Vinnakota, K., Kettenmann, H., Kotulska, K., Grajkowska, W., & Kaminska, B. (2013). Distinct roles of CSF family cytokines in macrophage infiltration and activation in glioma progression and injury response. *The Journal of Pathology*, *230*(3), 310–321. https://doi.org/10.1002/path.4192

Takacs, G. P., Kreiger, C. J., Luo, D., Tian, G., Garcia, J. S., Deleyrolle, L. P., Mitchell, D. A., & Harrison, J. K. (2022). Glioma-derived CCL2 and CCL7 mediate migration of immune suppressive CCR2+/CX3CR1+ M-MDSCs into the tumor microenvironment in a redundant manner. *Frontiers in Immunology*, *13*, 993444. https://doi.org/10.3389/fimmu.2022.993444

Tirosh, I., Izar, B., Prakadan, S. M., Wadsworth, M. H., Treacy, D., Trombetta, J. J., Rotem, A., Rodman, C., Lian, C., Murphy, G., Fallahi-Sichani, M., Dutton-Regester, K., Lin, J.-R., Cohen, O., Shah, P., Lu, D., Genshaft, A. S., Hughes, T. K., Ziegler, C. G. K., … Garraway, L. A. (2016). Dissecting the multicellular ecosystem of metastatic melanoma by single-cell RNA-seq. *Science (New York, N.Y.)*, *352*(6282), 189–196. https://doi.org/10.1126/science.aad0501

Tiwari, R. K., Singh, S., Gupta, C. L., & Bajpai, P. (2021). Microglial TLR9: Plausible Novel Target for Therapeutic Regime Against Glioblastoma Multiforme. *Cellular and Molecular Neurobiology*, *41*(7), 1391–1393. https://doi.org/10.1007/s10571-020-00925-z

Vakilian, A., Khorramdelazad, H., Heidari, P., Sheikh Rezaei, Z., & Hassanshahi, G. (2017). CCL2/CCR2 signaling pathway in glioblastoma multiforme. *Neurochemistry International*, *103*, 1–7. https://doi.org/10.1016/j.neuint.2016.12.013

Veleeparambil, M., Wang, C., Kessler, P. M., Sengupta, P., Das, S., Chakravarti, R., Willard, B., Sen, G. C., & Chattopadhyay, S. (2025). TLR9 signaling requires ligand-induced phosphorylation of two specific tyrosine residues by EGFR and Syk. *mBio*, e0027625. https://doi.org/10.1128/mbio.00276-25

Virtuoso, A., De Luca, C., Cirillo, G., Riva, M., Romano, G., Bentivegna, A., Lavitrano, M., Papa, M., & Giovannoni, R. (2022). Tumor Microenvironment and Immune Escape in the Time Course of Glioblastoma. *Molecular Neurobiology*, *59*(11), 6857–6873. https://doi.org/10.1007/s12035-022-02996-z

Wang, J., Li, X., Wang, K., Li, K., Gao, Y., Xu, J., Peng, R., Zhang, X., Zhang, S., Zhou, Y., Xu, S., & Zhang, J. (2024). CLEC7A regulates M2 macrophages to suppress the immune microenvironment and implies poorer prognosis of glioma. *Frontiers in Immunology*, *15*, 1361351. https://doi.org/10.3389/fimmu.2024.1361351

Yang, J., Yamashita-Kanemaru, Y., Morris, B. I., Contursi, A., Trajkovski, D., Xu, J., Patrascan, I., Benson, J., Evans, A. C., Conti, A. G., Al-Deka, A., Dahmani, L., Avdic-Belltheus, A., Zhang, B., Okkenhaug, H., Whiteside, S. K., Imianowski, C. J., Wesolowski, A. J., Webb, L. V., … Roychoudhuri, R. (2025). Aspirin prevents metastasis by limiting platelet TXA2 suppression of T cell immunity. *Nature*, *640*(8060), 1052–1061. https://doi.org/10.1038/s41586-025-08626-7

Yuan, R., Wang, J., Zhang, S., Xu, Z., & Song, L. (2025). Phosphofructokinase-1 redefined: A metabolic hub orchestrating cancer hallmarks through multi-dimensional control networks. *Journal of Translational Medicine*, *23*(1), 873. https://doi.org/10.1186/s12967-025-06897-2

Zawadzka, M., & Kaminska, B. (2005). A novel mechanism of FK506-mediated neuroprotection: Downregulation of cytokine expression in glial cells. *Glia*, *49*(1), 36–51. https://doi.org/10.1002/glia.20092

Zhang, L., Qu, X., & Xu, Y. (2024). Molecular and immunological features of TREM1 and its emergence as a prognostic indicator in glioma. *Frontiers in Immunology*, *15*, 1324010. https://doi.org/10.3389/fimmu.2024.1324010

Zhu, C., Chen, X., Liu, T.-Q., Cheng, L., Cheng, W., Cheng, P., & Wu, A.-H. (2024). Hexosaminidase B-driven cancer cell-macrophage co-dependency promotes glycolysis addiction and tumorigenesis in glioblastoma. *Nature Communications*, *15*(1), 8506. https://doi.org/10.1038/s41467-024-52888-0